THE JOURNAL OF PHYSICAL CHEMISTRY C

Article

pubs.acs.org/JPCC

Optical Properties of Ordered Self-Assembled Nanoparticle Arrays at Interfaces

Jack Paget,[†] Victoria Walpole,[†] Miquel Blancafort Jorquera,[†,¶] Joshua B. Edel,[†] Michael Urbakh,[‡] Alexei A. Kornyshev,*[,†] and Angela Demetriadou*[,†]

[†]Department of Chemistry, Imperial College London, London, SW7 2AZ, United Kingdom

[‡]School of Chemistry, Tel-Aviv University, Tel-Aviv, 69978, Israel

[¶]Faculty of Chemistry, Universitat de Barcelona, Marti i Franques, 1-11, 08028 Barcelona, Spain

Supporting Information

ABSTRACT: Nanoplasmonic metamaterials are rapidly finding uses in optical devices. Self-assembled soft matter optical nanostructures are straightforward to manufacture and are low cost, self-healing, and tunable. The simplest way to self-assemble such structures is to bring nanoparticles to interfaces where they can build lattices. While being simple to manufacture, these systems are difficult to model analytically. Here we develop an analytical model that is suitable for interfacial systems, that takes account of interactions of the nanoplasmonic structures at various interfaces and electrodes. The model is applicable to both thin-film and bulk electrodes, and it compares well with numerical calculations. On the basis of our model we propose designs suitable for simple surface-enhanced Raman scattering and optical mirror devices.

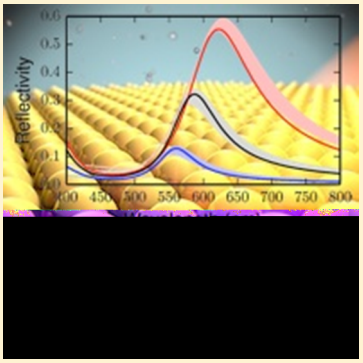

INTRODUCTION

Nanoplasmonic structures have been exploited for many centuries, and their use predates modern science.[1] Theoretical interest in nanoplasmonics has been growing over the past century since the fundamental work of Gustav Mie[2] and suggestion, in 1928, by Synge[3] that colloids could be used in sensing. In recent decades the ability to experimentally realize nanoplasmonic structures and potentially exploit their highly promising properties in optics, sensing, and detection has led to an explosion of scientific and engineering interest.[4] The promise of nanoplasmonics structures has not yet been fully realized, although they have been employed for detection, such as colorimetric[5,6] and surface enhanced Raman scattering (SERS).[7−9] Metal nanoparticles (NPs), whose size by definition is in the nanometer regime, have a plasmonic response in the ultraviolet, visible, and near-infrared region and are therefore most commonly used for such sensing purposes. The excitation of their plasmonic modes yields high field enhacement in the vicinity of each NP, enabling trace analyte detection.[7,10]

Many devices based on nanoplasmonic structures rely on top-down assembly techniques available only to solid-state devices.[11] Top-down approaches can however prove costly, time-consuming, and difficult to scale-up, which has led to other routes being developed. Self-assembly is one such route and has been found to be a promising approach to nanofabrication[12] capable of fabricating, in bulk, complex and unique nanoscaled metal structures,[13,14] previously not possible with top-down techniques. Although arguably self-assembly cannot provide the precision of top-down techniques, it does provide a cost efficient and easily scalable route toward devices. NPs self-assemble into arrays with some order at interfaces[15,16] such arrays have found applications in SERS sensing[7,17] and as the building blocks for nanocavity-based sensors.[8,18] The self-assembly of NPs at a solid/liquid interface can be directed by surface treatment to produce highly ordered two-dimensional arrays.[19] Assemblies of NPs at a liquid/liquid interface have long been suggested as potential liquid mirrors[20,21] and SERS sensors.[22] More recently it has been demonstrated that the NP population at an electrified liquid/liquid interface can be controlled with electric potential[23−26] or by salt concentration.[25−27] Any devices based on NP assemblies at a liquid/liquid interface benefit from a bottom up self-assembly and an ability to self-correct defects. These features have sparked a renewed interest in nanoplasmonic structures at liquid/liquid interfaces with a plasmon ruler[27] and multiphase multianalyte SERS sensor[7] being demonstrated at an oil/water interface, and the electrochemical modulation of SERS being studied at an electrified oil/water interface.[28]

Notwithstanding the broad range of applications for controlled NP self-assemblies, a problem arises when attempts are made to characterize these promising systems, especially when NPs are assembled at a liquid/liquid interface. When at the interface, experimental characterization is limited to X-ray

Received: July 17, 2014
Revised: September 4, 2014
Published: September 10, 2014

dx.doi.org/10.1021/jp5071192 | J. Phys. Chem. C 2014, 118, 23264−23273

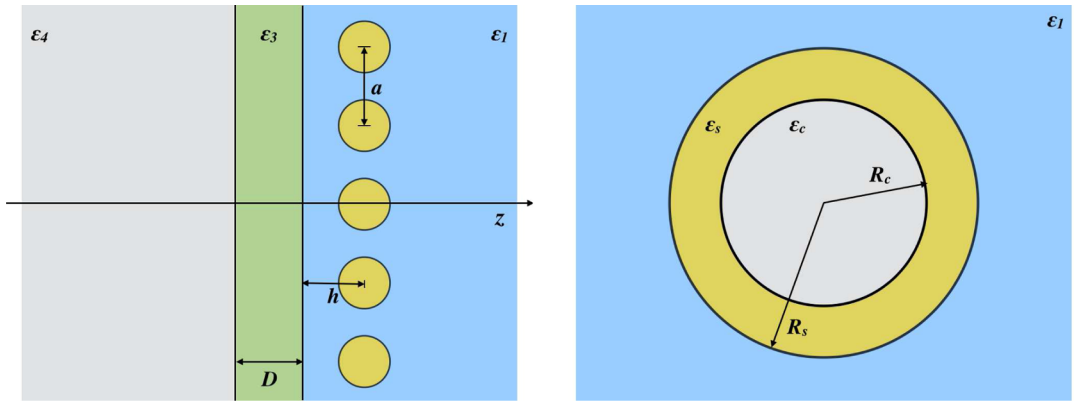

Figure 1. The system (a) is modeled as an array of NPs (b) at interfaces. The sketch of the system shown in (a) is of NPs with center-to-center spacing, a, disposed a distance h from a thin electrode. The NPs are in a medium with dielectric constant ε_1 from which the light is incident at an angle θ to the z-axis. The thin-film electrode is composed of a film of thickness D and dielectric constant ε_3 and a semi-infinite material of dielectric constant ε_4. The NPs are either monometallic NPs of radius R and dielectric constant ε_m or core−shell NPs (b) comprising a core of radius R_c and dielectric constant ε_c, and a shell of radius R_s and dielectric constant ε_s.

scattering[29] or measuring integral average properties, such as optical reflectivity[26,27,30] or electrical capacitance.[31,32] The difficulties in experimental characterization place increased importance on theoretical modelling of the nano structures or the understanding of their plasmonic modes and consequently the structures effect on the system's detection/sensing capabilities. Theories have been developed for the response of NPs at solid/liquid interfaces with exact solutions of Maxwell's equations possible for single[33] and multiple particle systems.[34] However, the NPs are maintained at a liquid/liquid interface by crossing the interface reducing the unfavourable contact between the immiscible liquids.[25,26,35] This crossing leads to a system with a three phase boundary, rendering an analytic solution to Maxwell's equations extremely challenging. This challenge is amplified by the fact that an array of NPs is required and that the precise position of the NPs at the interface is not known. Studies have shown order,[27] yet this order is short ranged and hence any model must be able to accommodate a disordered or only partially ordered array of NPs. The form of effective medium dipole approximation proposed can be extended to disordered systems.[36,37]

Approximating the multipole response of an NP by its dipole response is well-established in nanoplasmonics and known as the dipole approxmation (DA).[38] Here, we present a DA model combined with an effective medium theory, to describe the properties of arrays of NPs at various interfaces. The effective medum approach used differs from the more commonly used Maxwell−Garnett-like approaches in that the NPs can be spatially correlated.[30,36] The model presented is extremely flexible and capable of modeling multishell NPs, in a variety of interesting systems (liquid/liquid, liquid/solid, and liquid/thin-film interfaces). Herein, we seek to demonstrate the strength and flexibility of this effective medium DA by comparison with numerical calculations, for a range of systems pertinent to interfacial self-assembly.

DIPOLE APPROXIMATION FOR NPS AT INTERFACES

The NPs of interest for self-assembled optical devices typically have diameters much less than the wavelength of visible light ($2R \ll \lambda_{\text{visible}}$), and thus it can be assumed that they experience a uniform electric field in both time and space. As the electric field is uniform the necessity to solve the full set of Maxwell equations is removed, and we can consider the particles in the quasi-static limit by solving only static equation for the NP geometry. Moreover, since the particles are small we consider only the dominant dipole mode of the NP response excluding the higher order multipoles.[26,30,38] Thus, the model we present falls into the category of a quasi-static DA. To calculate the properties of a lattice of NPs, we consider each NP to act as a dipole scatterer in the presence of an external electric field.[36,37] The total electric field at each lattice point is the sum of the external field and the field due to all other radiating dipoles. By calculating the dipole moment, $\vec{p} = \hat{\alpha}(\vec{E}_0 + \hat{U}[-zp_z + 1/2(xp_x + yp_y)])$, of a dipole interacting with all others, we can elucidate the components of the polarizability tensor for an array of dipoles. Here, we consider NPs composed of isotropic materials with no off-diagonal components in their permittivity tensor, and thus the polarizability tensor for the NP layer α^0 has three elements: two parallel $\alpha_{\parallel}^0$ and one perpendicular $\alpha_{\perp}^0$ relative to the NP layer.

$$\alpha_{\parallel}^{0} = \frac{\alpha_{\parallel}}{1 - \frac{\alpha_{\parallel}}{2\varepsilon_1} U_{\parallel}} \tag{1}$$

$$\alpha_{\perp}^{0} = \frac{\alpha_{\perp}}{1 + \frac{\alpha_{\perp}}{\varepsilon_1} U_{\perp}} \tag{2}$$

The $\alpha_{\parallel,\perp}$ term is the polarizability of a single average NP in the array of particles, and for most cases this is an analytic function determined by solving Laplace's equations for a single NP. $U_{\parallel,\perp}$ arises from solving Laplace's equation in the geometry of interest to yield the dipole moment. The $U_{\parallel,\perp}$ term is dependent on the number of dielectric interfaces and becomes increasingly cubersome as the number of dielectric layers increases. The expressions for $U_{\parallel,\perp}$ (eqs 3 and A16 of the SI, respectively) were calculated using the image charge method to determine the potential of a point dipole.[39]

dx.doi.org/10.1021/jp5071192 | J. Phys. Chem. C 2014, 118, 23264−23273

$$U_{\parallel} = \sum_j \left[\frac{1}{a^3 |r_j|^{3/2}} - \gamma_{31} \left(\frac{1}{a^3 \left(\frac{4h^2}{a^2} + |r_j|^2 \right)^{3/2}} - \frac{12h^2}{a^5 \left(\frac{4h^2}{a^2} + |r_j|^2 \right)^{5/2}} \right) + \eta_{34}\eta_{43}\gamma_{13} \sum_{n=0}^{\infty} (\gamma_{13}\gamma_{43})^n \left(\frac{1}{a^3 \left(\frac{4(h + D(n+1))^2}{a^2} + |r_j|^2 \right)^{3/2}} - \frac{12(h + D(n+1))^2}{a^5 \left(\frac{4(h + D(n+1))^2}{a^2} + |r_j|^2 \right)^{5/2}} \right) \right] - \frac{1}{2} U_{\parallel}(|r_j| = 0) \quad (3)$$

The NP center-to-center distance is a. It is clear from eq 3 that $U_{\parallel,\perp}$ is $\propto (1/a)$, therefore at large separations the NPs do not interact with each other and instead behave as a collection of individual particles, $|r_j| = (x_i + y_j)^{1/2}$, and gives the position of the NPs in the lattice in the x,y-plane. The image charge terms in the expressions for $U_{\parallel,\perp}$ are $\propto (1/h^3)$ where h is the distance between the dielectric interface of mediums 2 and 3 and the center of the NP. The NP array parameters are shown in Figure 1. As the NPs are disposed further from the interface the contribution of the image charges is reduced. The image charge contribution is determined not only by h but also by the number of layers: (i) for NPs in a single medium there are no image charge interactions; (ii) with a single dielectric interface such as NPs at a liquid/liquid interface the image charge interactions take the form $\gamma_{ij} = ((\varepsilon_i - \varepsilon_j)/(\varepsilon_i + \varepsilon_j))$; and (iii) on increasing complexity to three interfaces which is a system resembling a thin-film electrode, the image interactions are governed by γ_{ij}, $\eta_{ij} = (\varepsilon_i/(\varepsilon_i + \varepsilon_j))$, and D the thickness of layer 2. The last term in eq 3 represents the self-interaction term between a dipole and its own image. Using eqs 1−3 the polarizability of a layer of NPs can be calculated for NPs in a medium, NPs at a dielectric interface, and NPs near almost any thin-film material.[40]

In the interests of brevity the term for $U_{\perp}$ can be found in the SI. The summation in j is taken over the lattice of dipoles. NPs are charged to repel each other and prevent agglomeration, so we assume a hexagonal lattice structure. This assumption is supported by experimental data.[27] The polarizability of the NP array can be used to calculate the SERS enhancement factor and other properties such as the effective scattering, absorption, and extinction cross-sectional areas. In this work we only consider the frequency dispersion of the dielectric permittivities of the NP and interface materials, thus we disregard any possible spatially dispersive or "non-local" effects. Non-local effects are known to cause a shift in the resonance peak[41−43] and may give rise to new peaks.[33] However, for the distances between NPs that we here consider and within the limits of applicability of the other approximations used, we can neglect non-local effects.[44,45]

In an effective medium approach the NP array can be considered as a homogeneous anisotropic film with effective dielectric properties determined by the dipolar response of the NP array. By considering the standard electrostatic boundary conditions at the interfaces between the NP layer and host medium, the effective dielectric permittivity tensor of the NP layer can be calculated.[26,30,46] This again has two parallel, $\varepsilon_{\parallel}$, and one perpendicular, $\varepsilon_{\perp}$, components, with the NP array properties manifesting through the effective polarizability of the NP layer. The NP layer is modeled as a system of point-like dipoles, these point-like dipoles form a two-dimensional array. The dielectric permittivity of a material is defined per unit volume, and therefore an effective thickness of the effective NP layer, d, must be introduced and is arbitrarily defined as d = 1 nm.[30]

$$\varepsilon_{\parallel} = 4\pi \frac{\alpha_{\parallel}^{0}}{a^2 d} + \varepsilon_1 \quad (4)$$

$$\varepsilon_{\perp} = \varepsilon_1 - \frac{1}{4\pi} \frac{\varepsilon_1^2 a^2 d}{\alpha_{\perp}^{0}} \quad (5)$$

Having determined a method for calculating the polarizability and effective dielectric permitivity of the NP array, we can proceed to estimate properties of the system. The scattering, extinction, and absorption cross sectional areas can be estimated from the polarizability as can the SERS enhancement factor $\eta = (7/4)|(\alpha_{\parallel}^{0}/R^3)|$.[36] The estimated dielectric permittivity allows calculation of the reflection spectrum among other properties for the layer of NPs. Herein we calculate the reflection spectrum for NP layers in a variety of configurations applicable to self-assembled systems. The reflection spectrum for an N-layered system is calculated using the T-matrix approach[47] as given by eq 6, where the standard Fresnel reflection coefficients are given by $r_{i,j}^{s} = (k_{i,\parallel} - k_{j,\parallel})/(k_{i,\parallel} + k_{j,\parallel})$ for s-polarized light and $r_{i,j}^{p} = (\varepsilon_{i,\parallel} k_{i,\perp} - \varepsilon_{j,\parallel} k_{j,\perp})/(\varepsilon_{i,\parallel} k_{i,\perp} + \varepsilon_{j,\parallel} k_{j,\perp})$ for p-polarized light. The phase shift, $\delta = e^{2ik_i d_i}$, where d_i is the thickness of layer i

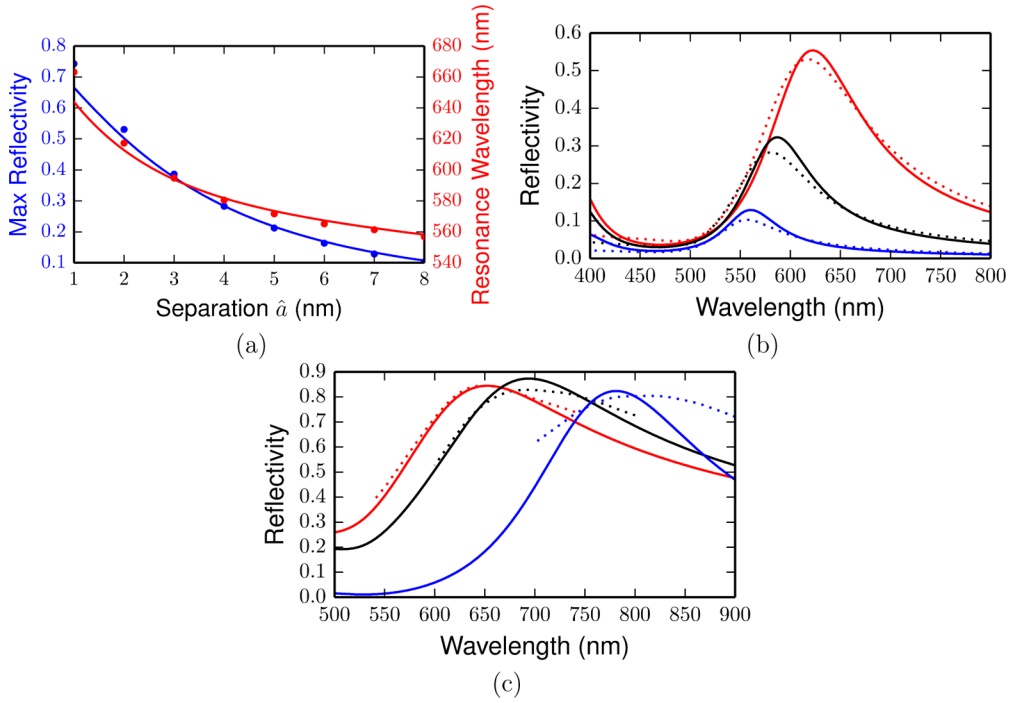

Figure 2. A comparison of the reflectivity of monolayers of gold NPs in water calcuated using the effective medium dipole approximation and numerical methods. In all cases the light is at normal incidence ($\theta = 0$) and the dielectric constant of water is $\varepsilon_{1,3,4} = 1.78$. For both numerical calculation (points) and the theoretical method (solid line) the dielectric constant of gold was taken from a fit to experimental data.[50] Plot (a) shows the position (blue) and magnitude (red) of the LSPR for monometallic $R = 8$ nm gold NPs in water across a range of surface coverages ($\Gamma = 1-0.46$, $a = 17-25$ nm, $\hat{a} = 1-8$ nm) and plot (b) shows the full spectrum for three surface coverages, $\Gamma = 0.892$ (red), 0.655 (black), and 0.462 (blue), for the same $R = 8$ nm monometallic gold NPs. Plot (c) shows the response of $R_s = 16$ nm core−shell NPs composing a silica core $\varepsilon_c = \varepsilon_{SiO_2} = 2.25$ in an array with $\Gamma = 0.722$ ($a = 38$ nm, $\hat{a} = 6$ nm) in water for varying shell thicknesses $R_c = 4$ nm (blue), 6 nm (black), and 8 nm (red).

In general, NPs are composed of n concentric dielectric or metallic layers.[4] Here we consider monomaterial ($n = 1$) and bimaterial ($n = 2$) NPs composed of one or two concentric layer(s) respectively, see Figure 1. Forming NPs composed of two concentric shells of different materials allows manipulation of the optical or chemical properties of the materials shifting for example the localised surface plasmon resonance (LSPR). The polarizability of bimaterial NPs is given by eq 7 where the NP is considered to be a sphere comprising a core of radius R_c constructed from a material with dielectric permittivity ε_c and covered by a shell of radius R_s formed from a material with dielectric permittivity ε_s. Under the electrostatic dipole approximation and neglecting plasmon hybridization,[49] the concentric spheres are considered as two distinct dipoles in two spheres of different sizes; this means that the polarizability given by eq 7 best describes bimaterial (referred to as core−shell) NPs built from materials with large dielectric contrast ($|\varepsilon_c - \varepsilon_s| \gg 1$). For monomaterial NPs $R_c = R_s = R$ and $\varepsilon_c = \varepsilon_s$ thus eq 7 reduces to the familiar dipole polarizability of a sphere $\alpha_\mu = R_{s,c}^3((\varepsilon_{s,c} - \varepsilon_2)/(\varepsilon_{s,c} + 2\varepsilon_2))$.

$$\alpha_\mu = R_s^3 \frac{(\varepsilon_s - \varepsilon_1)(\varepsilon_c + 2\varepsilon_s) + \left(1 - \left(\frac{R_c}{R_s}\right)^3\right)(\varepsilon_c - \varepsilon_s)(2\varepsilon_s + \varepsilon_1)}{(\varepsilon_s + 2\varepsilon_1)(\varepsilon_c + 2\varepsilon_s) + \left(1 - \left(\frac{R_c}{R_s}\right)^3\right)(\varepsilon_c - \varepsilon_s)(2\varepsilon_s - 2\varepsilon_1)} \quad (7)$$

To demonstrate the applicabilty of the DA effective medium approach, we first consider a system with no dielectric inhomogeneities, which would be equivalent to NPs at an interface between two materials with perfectly matched dielectric constants or an imaginery two-dimensional array "floating" in water. In this simple case $U_{\parallel} = U_{\perp}$ (eqs 3 and A16 of the SI) as both expressions are reduced to a single term. This form of $U_{\perp,\parallel}$ is the same as that presented in the early seminal work of Liebsch and Persson.[36,37] It has also been used to estimate the reflectivity of an NP array at a liquid/liquid interface in the context of a putative electrovariable mirror.[26] In the latter case an approximation was made effectively equating the small dielectric contrast between oil and water at optical frequencies to zero. Although the practical applications of the theoretical method in this form are limited, it is useful to explore how the theory captures the interparticle interactions without the additional complexity of dielectric inhomgenities and the associated image charge terms.

Monometallic gold NPs are frequently mooted as good candidates for optical devices based on plasmonics in the visible range. In Figure 2a,b we compare results of the theoretical method with those from numerical calculation[51] for monometallic gold NPs at varying surface coverages and normal incidence. The surface coverage $\Gamma = (2R_s + 2\mathcal{L})^2/a^2$ where $(2R_s + 2\mathcal{L})$ is the shortest possible center-to-center distance for NPs bearing stabilizing ligands of length $\mathcal{L}$, we consider $\mathcal{L} = 1$ nm. R_s is used in the case of core−shell NPs for monometallic NPs $R_s = R$. The dipole lattice constant, a, is the actual center-to-center separation of the NPs, and for clarity we also state the NP surface-to-surface separation, $\hat{a}$.

Figure 2a shows that both the position and magnitude of the NPs response at the LSPR are accurately predicted by the theoretical method. This plot also shows that as expected at shorter separations (or higher Γ) the theoretical method begins

dx.doi.org/10.1021/jp5071192 | J. Phys. Chem. C 2014, 118, 23264−23273

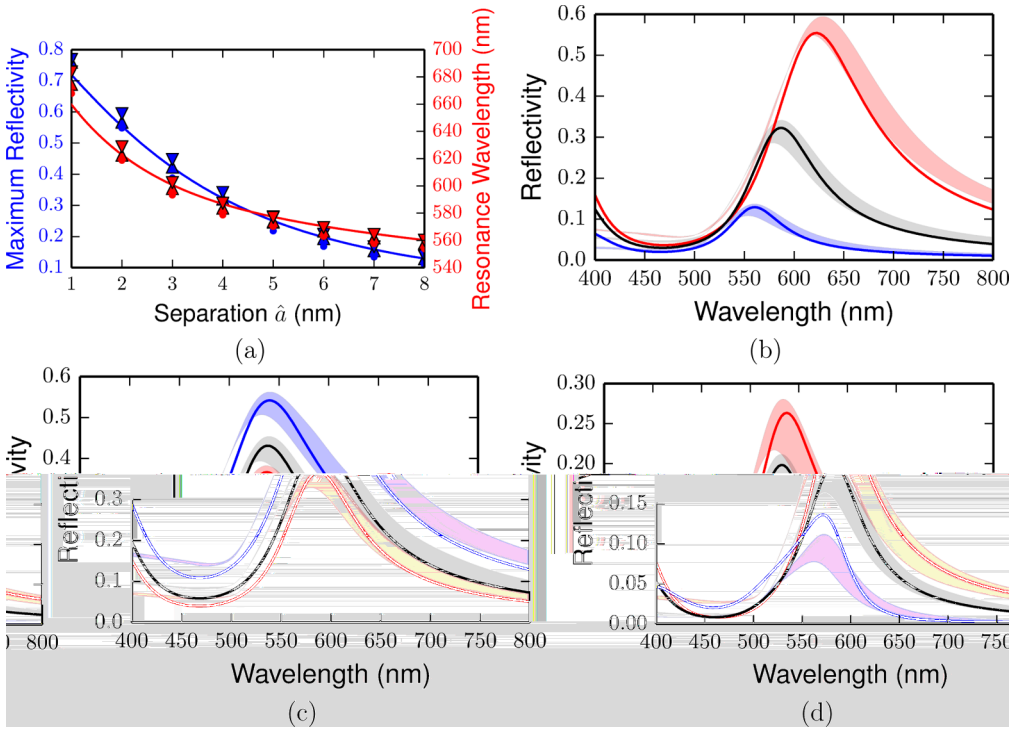

Figure 3. A comparison of the reflectivity calculated with the effective medium DA and numerical methods, from arrays of monometallic gold NPs at an oil/water interface. In all cases the NPs are R = 8 nm monometallic gold NPs at a water/dicholorethane. The dielectric constant of gold was calculated from a fit to experimental data;[50] the dielectric constant of water ε_1 = 1.78 and oil $\varepsilon_{3,4}$ = 2.03. Plot (a) shows the magnitude (blue) and position (red) of the LSPR for arrays with varying Γ. The numerical results are taken at three different interfacial positions, with NPs entirely in water (∇), mainly in water (Δ) and 50/50 crossing of the interface (●). Light is incident from water at normal (θ = 0°) incidence. Plot (b) shows the full spectrum for 3 surface coverages Γ = 0.892, 0.655, and 0.462 with a band showing the numerical results when the NPs are at different penetrations. Light is incident from water at normal (θ = 0°) incidence. Plot (c) shows the response for NPs entirely in water at Γ = 0.892 and varying angle of incidence θ = 45° (blue), 30° (black), and 15° (red) with the light always incident from water.

to breakdown overpredicting both the magnitude and position of the LSPR. This overprediction is most likely due to higher order multipole effects manifesting themselves due to the small distance between NPs; the next strongest multipole after the dipole is the quadrupole that damps the response of the system. At very large separations the theoretical method will also breakdown as the system can no longer be considered a homogeneous layer of scatterers interacting coherently with each other. This limit is however of little relevance to most potential applications; moreover it would be difficult to realize experimentally. Figure 2a,b shows the expected red-shift in the position of the LSPR as the NPs come closer together.[52] Figure 2b shows that the spectra produced by numerical and theoretical method agree with greater deviations at smaller Γ due to the breakdown of the layer homogenity approximation central to the effective medium approach. The deviation in behavior at short wavelengths (400−450 nm) maybe due to the reduced applicability of the DA at shorter wavelengths.[52]

Core−shell NPs created from silica cores with gold shells have great promise in sensing and optical applications. A sensor created from a silica core with a gold shell exhibits many of the beneficial properties of monometallic gold NPs while reducing the cost of the NPs by reducing the gold required. Moreover the thickness of the gold shell can be varied to shift the position of the LSPR. This could be used to create NPs for sensing with resonances closer to those of the most cost-efficient lasers. We considered silica core gold shell NPs with a constant surface coverage Γ = 0.72 (a = 20 nm, $\hat{a}$ = 4 nm) and shell radius (R_s = 16 nm) but with varying core radii (R_c = 8−14 nm) at normal incidence. As expected the LSPR frequency of the NP red shifts as R_c is increased, and interestingly even small changes in R_c appear to have a substantial effect on the LSPR frequency. The shift in the resonance is explained by "plasmon hybridization",[49] and the formation of NPs spanning the visible and near-infrared region by variation of R_c has been experimentally observed.[53,54] The theoretical method correlates well with the numerical calculations for all shell thicknesses considered, and it appears to more accurately coincide numerical calculations for thicker shells. As the thickness of the gold nanoshell decreases the approximation, required for the dipole theory, that the boundaries between gold and water and gold and silica have entirely independent resonances may not be appropriate. As with monometallic NPs the theoretical method successfully reproduces numerical calculation for the parameters we have considered. This serves to demonstrate that the combination of the effective medium and electrostatic dipole approach is accurate at capturing the physical interactions between NPs in an array.

NPs however will not spontaenously assemble to form layers in water or a single medium; instead they tend to form agglomerates or remain solitary in solution, depending on their electrostatic interactions. Self-assembling systems that build layers with some degree of order, and hence a coherent response, require a surface for assembly, and one such surface is an oil/water interface.

NP Arrays at Liquid/Liquid Interfaces. NPs assemble at an oil/water interface as they can cross the interface and block the unfavorable oil/water interfacial tension.[20,25,26,35] By

dx.doi.org/10.1021/jp5071192 | J. Phys. Chem. C 2014, 118, 23264−23273

blocking the interface the NPs find themselves in potential energy minima, and this energy well maintains the NPs at the interface. The use of monometallic silver or gold NPs, at a liquid/liquid interface, as mirrors has been suggested theoretically and demonstrated experimentally.[21,23,27] Although the magnitude of the reflectivity experimentally achieved thus far for a layer of single sized NPs has not yet met theoretical predictions, recent work involving NPs of different sizes promises the production of highly reflective self-healing liquid mirrors. The liquid/liquid interface can also be electrified by adding electrolytes to both the oil and water phase, and this opens the door to the possibility of reversible and even controlled assembly of NPs at the liquid/liquid interface by variation of electric potential across the interface.[23,25,26] Despite tentative experimental verification of reversible assemblies of small NPs (R = 1−2 nm) at liquid/liquid interfaces,[23] the idea of potential mediated controlled assembly is yet to be rigorously explored either theoretically or experimentally. We therefore focus on the optical properties of NP systems assuming that controlled spacing is achieveable.

To consider assemblies of NPs at a liquid/liquid interface analytically or quasi-analytically, we must work under the approximation that the NPs are entirely in either the oil or water phase. As most NPs are hydrophilic we consider the NPs as being located in the water phase assembling at the water/oil interface as if it were a liquid/solid interface. Numerically it is possible to consider the NP at varying levels of interfacial penetration, and this is represented by a band in Figure 3b−d and points in Figure 3, the NPs are either entirely in water (open symbol), crossing the interface but 2 nm more in water (crossed symbol) or exactly in the center of the interface (filled symbol); varying surface coverages are considered for R = 8 nm NPs at normal incidence. The theoretical model reproduces the numerical well for the surface coverages considered. Figure 3a shows that (viz. Figure 2) at higher Γ the theoretical model is closer to numerical result for the same system, and this is due to the fact that the homogenization used in the effective medium theory is more applicable at higher Γ, again countered by a greater deviation as $\Gamma \rightarrow 1$ in Figure 3a. To model the oil/water interface image, charge interactions must be included which increases the complexity of $U_{\parallel,\perp}$ in comparison to arrays in water that include the first three terms of and final (self-interaction) term of eqs 3 and A16 of the SI. The image charge method used appears to be sufficient to model the behavior of NPs at an oil/water interface, removing the need to resort to more complex models of polarizability for an NP crossing an interface. Although there is likely to be some local field effects arising from the interface that the theoretical model can not predict, it seems these effects do not manifest at the array level. Figure 3a demonstrates the broad applicability of the effective medium approach for the consideration of NPs self or otherwise assembled at a liquid/liquid interface with accurate prediction of both the position and magnitude of the coherent response at the LSPR.

Thus far, we have considered the coherent response of NPs at normal incidence, varying the angle of incidence causes differences in both the magnitude response and position of the LSPR. Figure 3c shows the response of an array of NPs with Γ = 0.655 (a = 20 nm, $\hat{a}$ = 4 nm) at varying angles of incidence (θ = 30°, 45°, 60°) for s-polarized light. In both theoretical and numerical calculations the position of the LSPR is not affected by the angle of incidence, however the magnitude of the response increases as the angle becomes more grazing. The theoretical method and numerical calculation are in good agreement across the spectrum in the case of s-polarized light. Again as Γ decreases the theoretical and numerical results begin to deviate slightly for the aforementioned reasons. Figure 3d is the same as Figure 3c, except that the light is p-polarized. When light is p-polarized oscillating dipoles are excited that are both parallel and perpendicular to the interface, which leads to a split peak; the peak visibile in Figure 3d arises from the a dipole oscillating in a direction parallel to the interface. Both theoretical and numerical results show this peak reducing in magnitude as the angle of incidence becomes more grazing. A second peak is also present in the spectrum in the near ultraviolet region, not shown in Figure 3 since it is outside of the visible region that we are interested in. This peak represents a dipole oscillating in a direction perpendicular to the interface and increases as the angle of incidence becomes more grazing. Although this peak is present in both the theoretical and numerical calculations there is a discrepancy of approximately 80 nm in its position. It is likely that the effective medium electrostatic dipole theory is less accurate in this region as the shorter wavelength means ($2R \rightarrow \lambda$), although it appears to be qualitatively correct. The theoretical method and numerical calculation both suggest that for s-polarized light reflection in the visible region can be increased by having a grazing angle of incidence. Since the elliptically polarized light that we experience is a combination of s- and p-polarized light, its probable that higher overall reflectivities in the visibile region could be achieved at more grazing incidence.

As well as mirror applications,[21,26] NPs assembled at an oil/water interface have found applications as SERS sensors.[22,28] We recently reported a highly sensitive SERS sensor based on gold NPs at an oil/water interface,[7] and more recently it has been reported that large dielectric NPs at an oil/water interface can provide a sensitive SERS sensor.[55] Such large NPs would be very stable at the interface and likely form highly ordered structures, however, although the theoretical method can be applied to dielectric NPs, the large (R > 200 nm) NPs suggested render a dipole approach inaccurate as $2R$ approaches λ. Solid surfaces also provide a route toward controlled and even tunable self-assembly by providing a surface for the NPs to assemble on and the possibility of voltage controlled assembly as many surfaces are conducting.[56]

NP Arrays at Liquid/Solid Interfaces. The effective medium DA model can be used for solid surfaces composed of any material. However, for metallic surfaces the dielectric contrast between water and the surface is large, meaning that the response is strongly dependent on the distance between the NP and the surface h.[30] The image charge terms decay as ($1/h^3$) and become negligible when $\hat{h} \gg R + \hat{a}$ with $\hat{h}$ and $\hat{a}$ being the NP electrode and NP−NP surface to surface separations, respectively. Transparent metal oxides such as indium tin oxide (ITO) have been suggested for optical applications due to the fact that they are both transparent in the visibile region and conductive.[26] Here we consider only an ITO surface which has a weak dielectric contrast with water in the visible region. As the dielectric contrast moderates the strength of any image a charge interactions a weak contrast renders the image charge terms and any dependence on h, negligible. We therefore consider NPs that are disposed only a few nm from the surface of the ITO which is an experimentally realizable[56] system and may provide an opportunity to tune the system by applying a potential to the conducting ITO. As with a liquid/liquid

dx.doi.org/10.1021/jp5071192 | J. Phys. Chem. C 2014, 118, 23264−23273

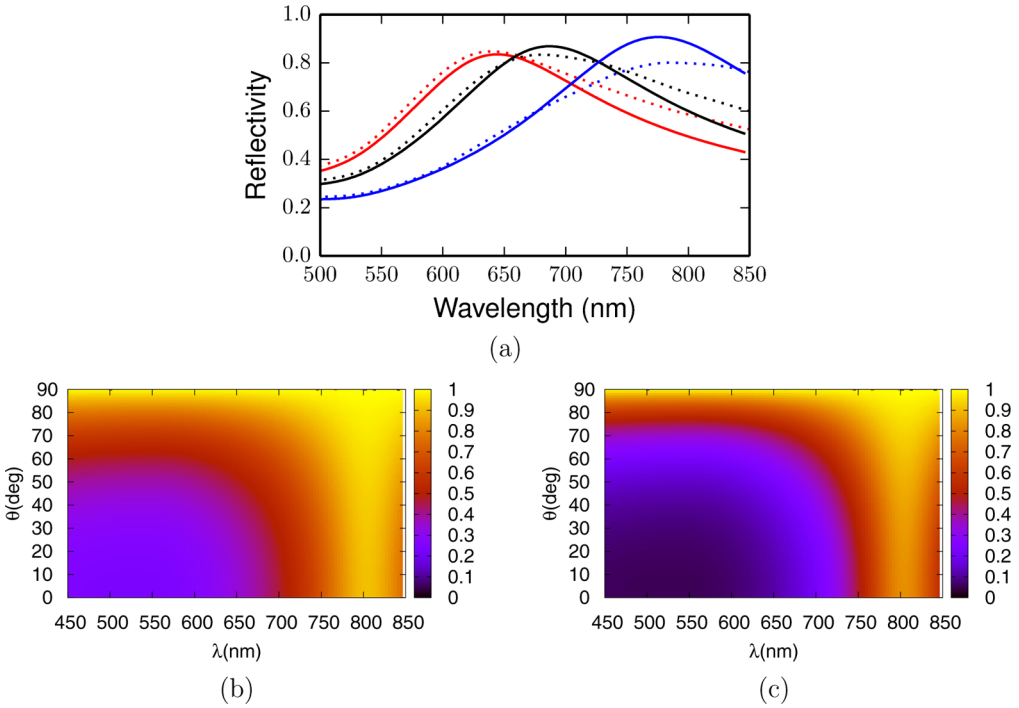

Figure 4. Comparing the response calculated with the effective medium DA and numerical methods of Au@SiO_2 NP arrays assembled on a semi-infinite ITO electrode for varying gold shell thicknesses. The NPs are diposed a distance h = 18 nm from the ITO electrode and are of radius R_s = 16 nm, the dielectric constant of silica is taken as ε_c = 2.25, and the dielectric permittivity of gold is fitted from experimental data.[50] The NP arrays are in water ε_1 = 1.78, $\varepsilon_{3,4}$ was determined from experimental data, and the light is incidence from water. The results of the theoretical method are shown as solid lines and numerical results are shown as dashed lines or points. Plot (a) shows the effect of varying shell thickness on an NP array with surface coverage Γ = 0.722 (a = 38 nm, $\hat{a}$ = 6 nm) for shell thicknesses R_c = 4 nm (blue), 6 nm (black), and 8 nm (red). Plot (b) shows the angular dependence of the response to s-polarized light R_c = 8 nm, and Γ = 0.722 (a = 38 nm, $\hat{a}$ = 6 nm) calculated using the effective medium dipole approximation. Plot (c) is the equivalent to plot (b) but for p-polarized light.

interface, here we consider only the first three and final term of $U_{\parallel,\perp}$ (eqs 3 and A16 of the SI).

As with the liquid/liquid interface, NPs will self-assemble at an ITO surface. We consider an array of core−shell NPs composing a silica core with a gold shell covering an ITO electrode with a surface coverage of Γ = 0.72 being illuminated at normal incidence. Figure 4a shows the effect of varying the core radius R_c, and as for the case of an NP array in water, changing the radius of the core leads to a red-shift in the resonance wavelength due to the coupling between cavity and shell plasmon modes, although this is moderated slightly by the blue-shift due to the hybridization of the plasmon resonance of the NP with the surface plasmon of the ITO electrode. As with the liquid/liquid interface, Figure 4 shows good agreement between the analytical and numerical theory with both predicting high reflectivities spanning the visibile and near-infrared spectrum. Figure 4b shows the reflection of s-polarized light at an angle of incidence, showing the same trend as for the normal incidence case, as only parallel plasmon modes are excited and the interaction between the NPs and the electrode is defined by the parallel effective polarizability. The p-polarized spectrum Figure 4c again arises due to excitation of parallel and perpendicular plasmon modes. The excitation of both modes gives split peaks in Figure 4c at larger core radii due to the opposing shifts in polarizabilities leading to two resonances being observed at close to the same wavelength. At larger core radii, a shoulder is observed in Figure 4; when considering core−shell NPs two plasmon resonances occur due to the interaction of the cavity plasmon with the shell plasmon. When an electrode is introduced into the system a second hybridization occurs with the two NP resonances, leading to the formation of three resonances. This peak represents this third resonance in Figure 4. However, a full consideration of the hybrid plasmons and comparison of the spectra with simulations are required to understand this fully. The reflection of both s- and p-polarized light (Figure 4b,c, respectively), incident at an oblique angle to the array and electrode, shows strongest reflection at the resonant wavelength and at large angles of incidence, with higher reflection achieved for s-polarized light than for p-polarized light at all wavelengths. Although ITO appears to be a promising candidate for optical applications, it is practically always found as a thin-film of metal oxide coating a glass coverslide, rather than as a semi-infinite slab.

To consider a thin-film of ITO or almost any other semiconducting material the full form of $U_{\perp,\parallel}$ (eqs 3 and A16 of the SI) must be considered. This more complex electrostatic calculation makes allowance for a film of a material of finite thickness. At large thicknesses ($D \gg 5R_s$) the D-dependent terms in eqs 3 and A16 of the SI tend to zero, and hence the ITO can be considered to be a semi-infinite slab in the electrostatic calculation, but not in the reflection calculation (eq 6). The dependence on the distance between the NPs and the electrodes is more complex, with the NP to electrode surface to surface distance needing to be $\hat{h} \gg R + \hat{a} + D$ before the image charge terms can be neglected. However, in this case the moderating factor of a low dielectric contrast between the glass, ITO, and water diminishes the strength of the image terms. Thin film ITO electrodes are conducting and are entirely transparent across the visible region and thus for the same

dx.doi.org/10.1021/jp5071192 | J. Phys. Chem. C 2014, 118, 23264−23273

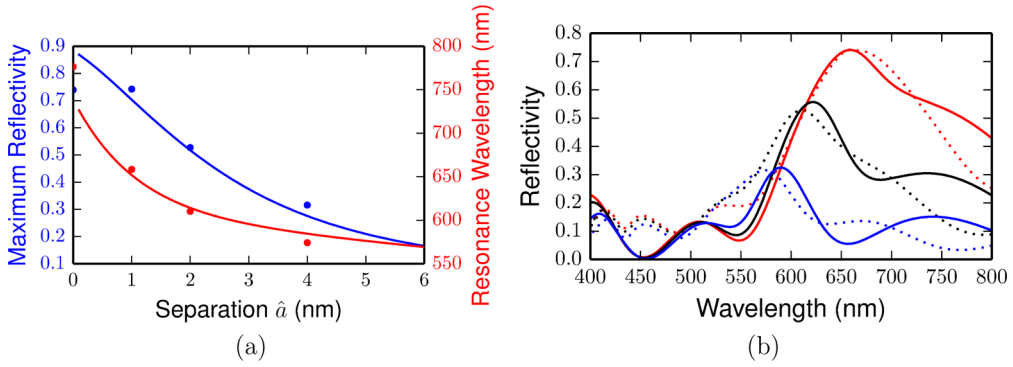

Figure 5. Optical response of monometallic gold NPs disposed 1 nm (h = 9 nm) from a thin-film ITO electrode, comparing the effective medium theory and numerical methods. The film has thickness D = 700 nm, comparing the effective medium dipole theory and numerical calculation. The dielectric constant of glass is taken to be ε_4 = 2.0 and the dielectric properties of ITO are calculated by a fit to experimental data. The dielectric properties of gold are taken from a fit to experimental data,[50] and the dielectric constant of water is taken as ε_1 = 1.78. The light is incident from water at with a normal angle of incidence relative to the ITO film. The results of theoretical model are shown as solid lines, and numerical results are shown as dashed lines or points. Plot (a) shows the position (blue) and magnitude (red) of the LSPR for monometallic R = 8 nm gold NPs in water across a range of surface coverages (Γ = 1−0.46, a = 17−25 nm, $\hat{a}$ = 1−8 nm), and plot (b) shows the full spectrum for three surface coverages, Γ = 0.892 (red), 0.655 (black), and 0.462 (blue), for the same R = 8 nm monometallic gold NPs.

reasons as a solid ITO electrode provide a route toward electrovariable optical devices.

The reflection spectra in Figure 5 show Fabry−Perot resonances due to the dielectric stack structure. The theoretical model and numerical calculations show good agreement in this case with the largest peak associated with the NP LSPR being close in position and magnitude. The shoulder seen on the resonance peak of the numerical results is more pronounced in the theoretical model, and the Fabry−Perot resonances in the 400−500 nm range are more pronounced than in the numerical theory. This is likely a combination of a slightly different fit to the experimentally obtained dielectric properties of the ITO and the method used to calculate the reflectivity. The shoulder on the resonance peak arises from the plasmonic interaction with the surface and the NPs; this suggests the theoretical model is not accurately predicting this interaction perhaps due to the dipole approximation. Qualtitatively however the spectra show good agreement for such a complex system and demonstrates the strength of the theoretical model. The results are presented in terms of reflection and show the strong coherent response of NPs assembled at various interfaces. If it were possible to control the assembly of NPs to form perfectly ordered arrays, then these results show that the optical properties of arrays could be manipulated to realize a wealth of applications.

Self-assembled arrays are cost-effective, unbreakable, and reuseable platforms to catalytic,[57,58] sensing[7] and optical applications.[24] The results presented so far are for perfectly ordered NP arrays, with the effective medium DA being shown as a suitable approach for exploring the properties of ordered NP arrays. It can be extended to partially or disordered arrays more like those obtained in experiment.[36,37]

CONCLUSIONS

We present a theoretical model based on a dipole approximation for NP arrays in a single medium and assembled at an interface or various electrodes. The model accurately represents the effective electromagnetic properties of the NP arrays and their interactions with interfaces, as demonstrated by the close agreement between numerical and theoretical calculation. The model accounts for both core−shell and monometallic NPs, with the former showing a significantly red-shifted resonance compared to the monometallic NPs. The image charge method is used to model the interaction of the NP array and the interface. The resulting model is applicable for both s- and p-polarized light at large oblique angles of incidence. The model is also used to calculate the plasmonic properties of monometallic and core−shell NP arrays assembled at both a semi-infinite and thin-film ITO electrode. ITO has the advantage of being transparent in the visible region, and therefore it is an ideal candidate for electrotunable SERS or mirror devices.

ASSOCIATED CONTENT

Supporting Information

Detailed outline of the DA effective medium model. This material is available free of charge via the Internet at http://pubs.acs.org/.

AUTHOR INFORMATION

Corresponding Authors

*E-mail: a.kornyshev@imperial.ac.uk.
*E-mail: a.demetriadou06@imperial.ac.uk.

Notes

The authors declare no competing financial interest.

ACKNOWLEDGMENTS

The authors are grateful to Vladimir Turek, Michael Cecchini, Cheuk Leung, and Colin Crick for useful discussions relating to the experimental possibilities in this area. The authors are thankful to Angharad Dare-Edwards for her advice on some of the more challenging aspects of the theoretical method. They also extend their thanks to Matthew Coles and Andrew Pearce for their last minute comments. A.A.K. and M.B.J. acknowledge the financial support of the Erasmus scheme at ICL. A.D. and A.A.K. completed this work with funding from the EU FP7 program Nanodetector project (NMP.2011.1.3-1). Part of this work was funded by an EPSRC grant (EP/L02098X/1) awarded to J.B.E. and A.A.K. M.U. acknowledges the support by the Israel Science Foundation grant no. 1109/09. J.B.E. also acknowledges the support of an E. R. C. Starting Investigator grant.

REFERENCES

(1) Freestone, I.; Meeks, N.; Sax, M.; Higgitt, C. The Lycurgus Cup-Roman Nanotechnology. *Gold Bull.* **2007**, *40*, 270−277.
(2) Mie, G. Beiträge zur Optik trüber Medien Speziell Kolloidaler Metallösungen. *Ann. Phys. (Berlin, Ger.)* **1908**, *25*, 377−445.
(3) Synge, E. H. A Suggested Model for Extending Microscopic Resolution into the Ultra-microscopic Region. *Philos. Mag.* **1928**, *6*, 356−362.
(4) Halas, N. J.; Lal, S.; Chang, W.-S.; Link, S.; Nordlander, P. Plasmons in Strongly Coupled Metallic Nanostructures. *Chem. Rev.* **2011**, *111*, 3913−3961.
(5) Gartia, M. R.; Hsiao, A.; Pokhriyal, A.; Seo, S.; Kulsharova, G.; Cunningham, B. T.; Bond, T. C.; liu, G. L. Colorimetric Plasmon Resonance Imaging Using Nano Lycurgus Cup Arrays. *Adv. Opt. Mater.* **2013**, *1*, 68−76.
(6) Park, J.; Yeo, J.-S. Colorimetric Detection of microRNA miR-21 Based on Nanoplasmonic Core-satellite Assembly. *Chem. Commun.* **2014**, *50*, 1366−1368.
(7) Cecchini, M. P.; Turek, V. A.; Paget, J.; Kornyshev, A. A.; Edel, J. B. Self-assembled Nanoparticle Arrays for Multiphase Trace Analyte Detection. *Nat. Mater.* **2013**, *12*, 165−171.
(8) Mahajan, S.; Abdelsalam, M.; Suguwara, Y.; Cintra, S.; Russell, A.; Bauberg, J.; Bartlett, P. Tuning Plasmons on Nano-structured Substrates for NIR-SERS. *Phys. Chem. Chem. Phys.* **2007**, *9*, 104−109.
(9) Galarreta, B. C.; Norton, P. R.; Lagugne-Labarthet, F. SERS Detection of Streptavidin/Biotin Monolayer Assemblies. *Langmuir* **2011**, *27*, 1494−1498.
(10) Edel, J. B.; Kornyshev, A. A.; Urbakh, M. Self-Assembly of Nanoparticle Arrays for Use as Mirrors, Sensors, and Antennas. *ACS Nano* **2013**, *7*, 9525−9532.
(11) Liu, M.; Ji, Z.; Shang, L. *Nanotechnology*; Wiley-VCH: New York, 2010.
(12) Ikkala, O.; ten Brinke, G. Functional Materials Based on Self-Assembly of Polymeric Supramolecules. *Science* **2002**, *295*, 2407−2409.
(13) Salvatore, S.; et al. Tunable 3D Extended Self-Assembled Gold Metamaterials with Enhanced Light Transmission. *Adv. Mater.* **2013**, *25*, 2713−2716.
(14) Demetriadou, A.; Oh, S. S.; Wuestner, S.; Hess, O. A Tri-helical Model for Nanoplasmonic Gyroid Metamaterials. *New J. Phys.* **2012**, *14*, 1367−2630.
(15) Grzelczak, M.; Vermant, J.; Furst, E. M.; Liz-Marza'n, L. M. Directed Self-assembly of Nanoparticles. *ACS Nano* **2010**, *4*, 3591−3605.
(16) Boker, A.; He, J.; Emrick, T.; Russell, T. P. Self-assembly of Nanopaticles at Interfaces. *Soft Matter* **2007**, *3*, 1231−1248.
(17) Yap, F. L.; Thoniyot, P.; Krishnan, S.; Krishnamoorthy, S. Nanoparticle Cluster Arrays for High-Performance SERS through Directed Self-Assembly on Flat Substrates and on Optical Fibers. *ACS Nano* **2012**, *6*, 2056−2070.
(18) Chen, A.; DePrince, A. E., III; Demortiére, A.; Joshi-Imre, A.; Shevchenko, E. V.; Gray, S. K.; Welp, U.; Vlasko-Vlasov, V. K. Self-assembled Large Au Nanoparticle Arrays with Regular Hot Spots for SERS. *Small* **2011**, *7*, 2365−2371.
(19) Yap, F. L.; Thoniyot, P.; Krishnan, S.; Krishnamoorthy, S. Evaporation-induced Self-assembly of Gold Nanoparticles into a Highly Organized Two-dimensional Array. *Phys. Chem. Chem. Phys.* **2002**, *4*, 6059−6062.
(20) Pickering, S. U. Emulsions. *J. Chem. Soc. D* **1907**, *91*, 2001−2021.
(21) Yogev, D.; Efrima, S. Novel Silver Metal Liquid Like Films. *J. Phys. Chem.* **1988**, *92*, 5754−5760.
(22) Gordon, K. C.; McGarvey, J. J.; Taylor, K. P. Enhanced Raman Scattering from Liquid Metal Films Formed from Silver Solutions. *J. Phys. Chem.* **1989**, *93*, 6814−6817.
(23) Su, B.; Abid, J.-P.; Fermin, D. J.; Girault, H. H. Reversible Voltage-Induced Assembly of Au Nanoparticles at Liquid Liquid Interfaces. *J. Am. Chem. Soc.* **2004**, *126*, 915−919.
(24) Bucaro, M. A.; Kolodner, P. R.; Taylor, J. A.; Sidorenko, A.; Aizenberg, J.; Krupenkin, T. N. Tunable Liquid Optics: Electrowetting-Controlled Liquid Mirrors Based on Self-Assembled Janus Tiles. *Langmuir* **2009**, *25*, 3876−3879.
(25) Flatté, M. E.; Kornyshev, A. A.; Urbakh, M. Understanding Voltage-induced Localization of Nanoparticles at a Liquid-Liquid Interface. *J. Phys.: Condens. Matter* **2008**, *20*, 073102−073102.
(26) Flatté, M. E.; Kornyshev, A. A.; Urbakh, M. Electrovariable Nanoplasmonics and Self-Assembling Smart Mirrors. *J. Phys. Chem. C* **2010**, *114*, 1735−1747.
(27) Turek, V. A.; Cecchini, M. P.; Paget, J.; Kucernak, A. R.; Kornyshev, A. A.; Edel, J. B. Plasmonic Ruler at the Liquid Liquid Interface. *ACS Nano* **2012**, *6*, 7789−7799.
(28) Booth, S. G.; Cowcher, D. P.; Goodacre, R.; Dryfe, R. A. W. Electrochemical Modulation of SERS at the Liquid/Liquid Interface. *Chem. Commun.* **2014**, *50*, 4482−4484.
(29) Kubowicz, S.; Hartmann, M. A.; Daillant, J.; Sanyal, M. K.; Agrawal, V. V.; Blot, C.; Konovalov, O.; Möhwald, H. Gold Nanoparticles at the Liquid-Liquid Interface: X-ray Study and Monte Carlo Simulation. *Langmuir* **2009**, *25*, 952−958.
(30) Kornyshev, A. A.; Marinescu, M.; Paget, J.; Urbakh, M. Reflection of Light by Metal Nanoparticles at Electrodes. *Phys. Chem. Chem. Phys.* **2012**, *14*, 1850−1859.
(31) Younan, N.; Hojeij, M.; Ribeaucourt, L.; Girault, H. Electrochemical Properties of Gold Nanoparticle Assemblies at Polarised Liquid Liquid Interfaces. *Electrochem. Commun.* **2010**, *12*, 912−915.
(32) Marinescu, M.; Urbakh, M.; Kornyshev, A. A. Voltage Dependent Capacitance of Metallic Nanoparticles at Liquid/Liquid Interfaces. *Phys. Chem. Chem. Phys.* **2011**, *14*, 1371−1380.
(33) Ruppin, R. Optical Absorption by a Small Sphere Above a Substrate with Inclusion of Non-local Effects. *Phys. Rev. B* **1992**, *45*, 11290−11215.
(34) Tang, V.; Dormale, B. Optical Absorption in Overcoats of Nanoparticle Arrays on a Metallic Substrate. *Plasmonics* **2011**, *6*, 195−200.
(35) Reincke, F.; Kegel, W. K.; Zhang, H.; Nolte, M.; Wang, D.; Vanmaekelbergh, D.; Möhwald, H. Understanding the Self-assembly of Charge Nanoparticles at the Water/Oil Interface. *Phys. Chem. Chem. Phys.* **2006**, *8*, 3828−3835.
(36) Liebsch, A.; Persson, B. N. J. Optical Properties of Small Metallic Particles in a Continuous Dielectric Medium. *J. Phys. C: Solid State Phys.* **1983**, *16*, 5375−5391.
(37) Persson, B. N. J.; Liebsch, A. Optical Properties of Two-dimensional Systems of Randomly Distributed Particles. *Phys. Rev. B* **1983**, *28*, 4247−4254.
(38) Yurkin, M. A.; Hoekstra, A. G. The Discrete Dipole Approximation: an Overview and Recent Developments. *J. Quant. Spectrosc. Radiat. Transfer* **2007**, *106*, 558−589.
(39) Barrera, R. G.; Guzmán, O.; Balaguer, B. Point Charge in a Three-dielectric Medium with Planar Interfaces. *Am. J. Phys.* **1978**, *46*, 1172−1179.
(40) $|\gamma_{12}\gamma_{32}| < 1$, otherwise the summation over n diverges.
(41) McMahon, J. M.; Gray, S. K.; Schatz, G. C. Nonlocal Optical Response of Metal Nanostructures with Arbitrary Shape. *Phys. Rev. Lett.* **2009**, *103*, 097403−097407.
(42) Pack, A.; Hietschold, M.; Wannemacher, R. Failure of Local Mie Theory: Optical Spectra of Colloidal Aggregates. *Opt. Commun.* **2001**, *194*, 277−287.
(43) McMahon, J. M.; Gray, S. K.; Schatz, G. C. Calculating Nonlocal Optical Properties of Structures with Arbitrary Shape. *Phys. Rev. B* **2010**, *82*, 035423−035435.
(44) GarciadeAbajo, F. J. Nonlocal Effects in the Plasmons of Strongly Interacting Nanoparticles, Dimers, and Waveguides. *J. Phys. Chem. C* **2008**, *112*, 17983−17987.
(45) Mal'shukov, A. G. Far Infra-red Absorption in Small Metallic Particles Non-local Theory. *Solid State Commun.* **1982**, *44*, 1257−1260.

(46) Bagchi, A.; Barrera, R. G.; Fuchs, R. Local-field Effect in Optical Reflectance from Adsorbed Overlayers. *Phys. Rev. B* **1982**, *25*, 7086−7096.
(47) Born, M.; Wolf, E. *Principles of Optics: Electromagnetic Theory of Propagation, Interference and Diffraction of Light*; Pergamon Press: Oxford, U.K., 1964.
(48) Draine, B. T.; Flatau, P. J. Discrete-dipole Approximation for Scattering Calculations. *J. Opt. Soc. Am. A* **1994**, *11*, 1491−1499.
(49) Prodan, E.; Nordlander, P. Plasmon Hydridization in Spherical Nanoparticles. *J. Chem. Phys.* **2004**, *120*, 5444−5454.
(50) Johnson, P. B.; Christy, R. W. Optical Constants of the Noble Metals. *Phys. Rev. B* **1972**, *10*, 79−83.
(51) A commercial-grade simulator based on the finite-difference time-domain method was used to perform the calculations.[59,60]
(52) Maier, S. A. *Plasmonics: Fundamentals and Applications*; Springer: New York, 2007.
(53) Quyen, T. T. B.; Su, W.-N.; Chen, K.-J.; Pan, C.-J.; Rick, J.; Chang, C.-C.; Hwang, B.-J. Au@SiO_2 Core/Shell Nanoparticle Assemblage used for Highly Sensitive SERS-Based Determination of Glucose and Uric Acid. *J. Raman Spectrosc.* **2013**, *4*, 1671−1677.
(54) Lu, L.; Sun, G.; Zhang, H.; Wang, H.; Xi, S.; Hu, J.; Tian, Z.; Chen, R. Fabrication of Core-shell Au-Pt Nanoparticle Film and its Potential Application as Catalysis and SERS Substrate. *J. Mater. Chem.* **2004**, *14*, 1005−1009.
(55) Rodreiguez, I.; Shi, L.; Lu, X.; Korgel, B. A.; Alvarez-Puebla, R. A.; Meseguer, F. Silicon Nanoparticles as Raman Scattering Enhancers. *Nanoscale* **2014**, *6*, 5666−5670.
(56) Zhang, K.; Wei, J.; Zhu, H.; Ma, F.; Wang, S. Electrodeposition of Gold Naoparticles Arrays on ITO Glass as Electrode with High Catalytic Activity. *Mater. Res. Bull.* **2013**, *48*, 1338−1341.
(57) Du, Y.; Wang, C. Preparation Ru, Bi Monolayer Modified Pt Nanoparticles as the Anode Catalyst for Methanol Oxidation. *Mater. Chem. Phys.* **2009**, *113*, 927−932.
(58) Gong, K.; Su, D.; Adzic, R. R. Platinum-Monolayer Shell on AuNi0.5Fe Nanoparticle Core Electrocatalyst with High Activity and Stability for the Oxygen Reduction Reaction. *J. Am. Chem. Soc.* **2010**, *132*, 14364−14366.
(59) Lumerical Solutions, Inc. http://www.lumerical.com/tcad-products/fdtd/ (accessed: July 16, 2014).
(60) Computer Simulation Technology. https://www.cst.com/Products (accessed: July 16, 2014).